Available online at www.sciencedirect.com
SCIENCE DIRECT
Planetary and Space Science 54 (2006) 1024–1032
Planetary and Space Science
www.elsevier.com/locate/pss

E ring dust sources: Implications from Cassini's dust measurements

Frank Spahn[a,*], Nicole Albers[d], Marcel Hörning[a], Sascha Kempf[b], Alexander V. Krivov[c], Martin Makuch[a], Jürgen Schmidt[a], Martin Seiß[a], Miodrag Sremčević[d]

[a]*Universität Potsdam, Institut für Physik, Nichtlineare Dynamik, Am Neuen Palais 10, Potsdam, Germany*
[b]*Max-Planck-Institut für Kernphysik, Heidelberg, Germany*
[c]*Astrophysikalisches Institut und Universitäts-Sternwarte, Friedrich-Schiller-Universität Jena, Germany*
[d]*Laboratory of Atmospheric and Space Physics, University of Colorado, Boulder, USA*

Received 2 December 2005; accepted 4 April 2006
Available online 21 July 2006

Abstract

The Enceladus flybys of the Cassini spacecraft are changing our understanding of the origin and sustainment of Saturn's E ring. Surprisingly, beyond the widely accepted dust production caused by micrometeoroid impacts onto the atmosphereless satellites (the impactor-ejecta process), geophysical activities have been detected at the south pole of Enceladus, providing an additional, efficient dust source. The dust detector data obtained during the flyby E11 are used to identify the amount of dust produced in the impactor-ejecta process and to improve related modeling [Spahn, F., Schmidt, J., Albers, N., Hörning, M., Makuch, M., Seiß, M., Kempf, S., Srama, R., Dikarev, V.V., Helfert, S., Moragas-Klostermeyer, G., Krivov, A.V., Sremčević, M., Tuzzolino, A., Economou, T., Grün, E., 2006. Cassini dust measurements at Enceladus: implications for Saturn's E ring. Science, in press]. With this, we estimate the impact-generated dust contributions of the other E ring satellites and find significant differences in the dust ejection efficiency by two projectile families—the E ring particles (ERPs) and the interplanetary dust particles (IDPs). Together with the Enceladus south-pole source, the ERP impacts play a crucial role in the inner region, whereas the IDP impacts dominate the particle production in the outer E ring, possibly accounting for its large radial extent. Our results can be verified in future Cassini flybys of the E ring satellites. In this way poorly known parameters of the dust particle production in hypervelocity impacts can be constrained by comparison of the data and theory.

PACS: 94.10.Nh; 96.30.wr

Keywords: Saturn; Enceladus; E ring; Dust dynamics

1. Introduction

The E ring of Saturn extends from the orbit of the moon Mimas at 3 Saturnian radii ($R_\hbar = 60,268$ km) to Titan at $21R_\hbar$. It consists of icy dust grains of sizes $\approx 0.3,\ldots,3\,\mu$m in radius (Nicholson et al., 1996). The balance between the particle creation at Enceladus and to a lesser degree at the other satellites embedded in the E ring, and their annihilation in impacts on the same bodies and Saturn's A ring is responsible for the maintenance of this large dust complex. The particle creation process as well as their dynamics constrain the relatively narrow size range of particles that can stay in the ring (Showalter et al., 1991; Horányi et al., 1992).

Ejection of material by impacting projectiles (hereafter impactor-ejecta process) has been considered to be the most efficient process able to lift off particles into orbit around Saturn. The major impactor families are E ring particles (hereafter ERPs) and interplanetary dust particles (henceforth IDPs). However, it has not been clear which of both impactor types dominates the ring material supply. Hamilton and Burns (1994) discussed a self-sustainment of the E ring, but there are energetic arguments in favor of an additional support by IDP-projectile ejecta. Different IDP populations have been studied by Colwell (1993). His results have been used to predict the outcome of measurements of the cosmic dust analyzer (CDA) and to

*Corresponding author.
E-mail address: fspahn@agnld.uni-potsdam.de (F. Spahn).

0032-0633/$ - see front matter © 2006 Elsevier Ltd. All rights reserved.
doi:10.1016/j.pss.2006.05.022

discriminate between different impactor populations—the ERPs and IDPs (Spahn et al., 1999).

The view on the balance of the E ring matter has changed drastically when recently the high-rate detector (HRD) of the CDA uncovered an additional, efficient dust source near the south pole during the flyby E11 of the Cassini spacecraft with Enceladus on July 14th, 2005. A suite of Cassini experiments, infrared instruments (CIRS, VIMS), the neutral mass spectrometer (INMS), the magnetospheric imaging instrument (MIMI), the ultraviolet imaging spectrometer (UVIS), and the Cassini cameras (ISS), provided hints for geophysical activities at the south pole of Enceladus. The HRD has also registered at least five times more dust originating at the south pole than motes released in an impactor-ejecta process (Spahn et al., 2006). This region of the satellite is characterized by unusually high temperatures (>90 K compared to 70 K expected by solar irradiation) measured by CIRS and VIMS (Brown et al., 2006; Spencer et al., 2006), and clear signs of a geophysically active surface, the so-called "tiger-stripes", detected by the Cassini cameras—showing locally even higher temperatures >100 K. The data of ISS, UVIS, MIMI and INMS (Porco et al., 2006; Hansen et al., 2006; Jones et al., 2006; Waite Jr. et al., 2006) have found neutral gas escaping Enceladus' south pole.

In this paper, we investigate the dust production at all E ring satellites based on the results of the HRD/CDA measurements near Enceladus obtained during the E11 flyby (Spahn et al., 2006). The impactor-ejecta contribution of dust at Enceladus found with these measurements is used to calculate the impact-ejecta generated dust production at the satellites Mimas, Tethys, Dione and Rhea. For this purpose, it is reasonable to assume that the dust production at these moons is dominated by the impactor-ejecta process. With this assumption the efficiencies of the dust ejection by the different impactor families—ERPs or IDPs—are estimated. If there were significant differences in the related dust productions, future Cassini flybys of these satellites would allow us to distinguish between the dust contributions caused by IDPs and ERPs, so that their role in sustaining the E ring can be judged.

The paper is organized as follows. In Section 2 the physics of the impactor-ejecta process, driven by the different impactor families, is summarized. Dust contributions coming from different E ring satellites are derived and discussed in Section 3. Conclusions are drawn in Section 4.

2. Sources of E ring dust

The dust production processes at source satellites in the E ring provide the initial conditions for the dust particle dynamics governing the subsequent "life" of the dusty motes until they hit sinks—often their own sources, or the main rings. The balance between creation and removal of dust as well as the dynamical evolution of the grains between their "birth" and "death" determine largely the appearance of a dust ring. The major goal of this paper is to evaluate the dust production at the satellites embedded in the E ring based upon recent results of the Cassini mission at Saturn.

Observations (Showalter et al., 1991) and dynamical studies (Horányi et al., 1992) have convincingly pointed to Enceladus as the main source of the E ring of Saturn. The dust measurements performed during the flyby E11 of Cassini with Saturn on July 14, 2005, revealed that at least 85% of the grains are generated near Enceladus' south pole (Spahn et al., 2006), in geophysical processes (see Fig. 3). The remaining 15% of the dust rate detected by the HRD pose an upper limit on the dust creation rate in the impactor-ejecta process at Enceladus. It is plausible to assume that the impactor-ejecta process is also active at all other E ring satellites. In this paper we estimate the relative contributions of the dust production by the two projectile families at these satellites. To this aim in the following subsection we briefly summarize the physics of the impactor-ejecta mechanism.

2.1. The impactor-ejecta process

A common process of dust creation in the solar system is hypervelocity impacts of micrometeoroids onto surfaces of atmosphereless bodies—planets, asteroids, comets, satellites, ring particles, etc. Fig. 1 illustrates this mechanism schematically. A hypervelocity projectile may release considerably more material than its own mass. This cosmic erosion gave rise to speculations about the existence of dust rings around Mars (Soter, 1971), which still escape their discovery (see Showalter et al., 1991; Krivov et al., 2003; Makuch et al., 2006). Furthermore, such impacts play a major role in creating and sustaining circumplanetary dust rings (Hamilton and Burns, 1994; Showalter, 1998) and also dust clouds enveloping planetary satellites lacking a gas atmosphere (Krivov et al., 2003; Sremčević et al., 2003).

A quantitative description of the impactor-ejecta mechanism from first physical principles is complicated.

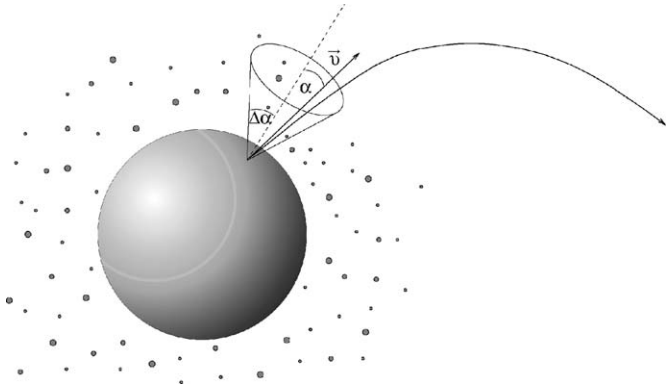

Fig. 1. Sketch of the impactor-ejecta model. An energetic projectile has hit the surface of a satellite, creating ejecta which leave the surface with the speed $\vec{v}$ in a cone of opening angle $\Delta\alpha$. The dashed line indicates the normal to the surface at the position of the impact.

Therefore, the following argumentation is mainly based on experimental data (Koschny and Grün, 2001) or dimensional analyses (Housen et al., 1983; Housen, 1991) reviewed in detail by Krivov et al. (2003). We recapitulate the most important relations characterizing the impactor-ejecta process, specified for Enceladus so that their validity can be judged with the Cassini HRD data. Then, we focus on the spatial dependencies of these relations in order to apply them to the other E ring moons.

Essential for the efficiency of cosmic erosion is the mass flux of the impacting projectiles defined as

$$F_{\mathrm{imp}} = \langle m_{\mathrm{imp}}\rangle n_{\mathrm{imp}}(r)\langle v_{\mathrm{imp}}\rangle(r), \tag{1}$$

with the mass of the impactors m_{imp}, the related number density $n_{\mathrm{imp}}(r)$ and impact velocity $\langle v_{\mathrm{imp}}\rangle(r)$ at the target satellite r. The mass production rate caused by the impacting projectiles is then defined by

$$M^{+} = F_{\mathrm{imp}}\, YS, \tag{2}$$

with the cross section of the source satellite $S = \pi R^2$. The yield Y is the fraction of the ejected mass to that of the projectile (IDP, ERP). Laboratory experiments (Koschny and Grün, 2001) suggest the relation (in SI units)

$$Y = 2.64 \times 10^{-5}\, \mathrm{m}_{\mathrm{imp}}^{0.23} v_{\mathrm{imp}}^{2.46}, \tag{3}$$

for icy surfaces. This choice of yield Y assumes similar surface properties. We assume a power law for the cumulative size distribution in order to obtain the total number of ejected particles larger than a certain radius s

$$N^{+}(>s, r) = \frac{3-\gamma}{\gamma}\frac{F_{\mathrm{imp}}\, YS}{m_{\max}}\left(\frac{s_{\max}}{s}\right)^{\gamma} \tag{4}$$

as a function of the distance r from Saturn. For the mass distribution index γ we choose $\gamma = 12/5$ (Krivov et al., 2003), but different values have been applied as e.g. $\gamma = 2.1$ at Enceladus (Juhász and Horányi, 2002). The parameters $s_{\max}$ and thus $m_{\max}$ are radii and masses characteristic for the impactor's family. The velocities of the N^{+} particles are distributed according to a power law (Krivov et al., 2003)

$$f_v = \frac{\beta-1}{v_0}\left(\frac{v}{v_0}\right)^{-\beta}\Theta[v - v_0], \tag{5}$$

with the normalization

$$\int_0^{\infty} f_v(v) = 1, \tag{6}$$

where $\Theta(x)$ denotes the Heaviside function. The slope of the velocity distribution lies in the range $\beta \in (2, 3)$, where $\beta \approx 2$ is suitable for regolith and the steeper slope ($\beta \approx 3$) applies to solid surfaces.

The parameter v_0 ensures the convergence of the integral and is, together with the yield Y, source of rather large uncertainties of N^{+}. Both values, v_0 and Y, depend on each other according to

$$\frac{K_{\mathrm{e}}}{K_{\mathrm{i}}} = Y\frac{\beta-1}{3-\beta}\left(\frac{v_0}{v_{\mathrm{imp}}}\right)^2\left\{\left(\frac{v_0}{v_{\max}}\right)^{\beta-3} - 1\right\} \quad \text{for } \beta \neq 3,$$

$$\frac{K_{\mathrm{e}}}{K_{\mathrm{i}}} = 2Y\left(\frac{v_0}{v_{\mathrm{imp}}}\right)^2 \ln\frac{v_{\max}}{v_0} \quad \text{for } \beta = 3. \tag{7}$$

The ratio $K_{\mathrm{e}}/K_{\mathrm{i}}$ between the kinetic energies of the ejecta K_{e} and the impactors K_{i}, respectively, depends on the mean impact speeds and projectile masses. For instance, one obtains for the IDPs $K_{\mathrm{e}}/K_{\mathrm{i}} \approx 0.3$ and for the E ring impactors $K_{\mathrm{e}}/K_{\mathrm{i}} < 0.05$ (Krivov et al., 2003).

The three-body escape velocity of the source moon of radius R and mass M is

$$v_{\mathrm{esc}} = \sqrt{2GM\left(\frac{1}{R} - \frac{1}{h_{\mathrm{Hill}}}\right)}, \tag{8}$$

where $h_{\mathrm{Hill}} = r\sqrt[3]{M/3(M_{\hbar} + M)}$ denotes the radius of the moon's Hill sphere with Saturn's mass $M_{\hbar}$. Now we can calculate the fraction

$$N_{\mathrm{esc}}^{+}(>v_{\mathrm{esc}}, >s, r) = (v_0/v_{\mathrm{esc}})^{\beta-1} N^{+}(>s, r) \tag{9}$$

of ejecta having velocities larger than the three-body escape velocity, i.e. providing an estimate for the efficiency of the dust source located at the distance r from Saturn. Similarly, the total mass rate of escaping particles is

$$M_{\mathrm{esc}}^{+}(>v_{\mathrm{esc}}, r) = (v_0/v_{\mathrm{esc}})^{\beta-1} M^{+}(r). \tag{10}$$

To account for anisotropies of ejection efficiency the distribution (9) can be folded with an angular distribution of positions on the satellite surface (Sremčević et al., 2003). In this way it is possible to simulate isolated dust sources, which has, for example, led to the identification of the south-pole source at Enceladus in the CDA data (Spahn et al., 2006).

In the following we will estimate the respective $N^{+}(r)$ for the IDPs and ERPs. While for the IDPs the dependence of N^{+} on radial distance from Saturn is caused by the varying strength of gravitational focusing by the planet, the production rate of particles in impacts of ERPs varies strongly with the projectile density, and thus, a model of the whole ring is necessary in order to estimate N^{+} for the ERPs. These differences in the dust production efficiencies should be detectable with the CDA in future flybys of Cassini at E ring moons.

2.2. Interplanetary dust projectiles—IDPs

The mass flux of IDPs at Saturn (Divine, 1993)

$$F_{\mathrm{imp}}^{(\infty)} = 1.8 \times 10^{-16}\,\mathrm{kg\,m^{-2}\,s^{-1}} \tag{11}$$

and its corresponding velocity relative to Saturn

$$v_{\mathrm{imp}}^{(\infty)} = 9.5\,\mathrm{km\,s^{-1}} \tag{12}$$

are modified by the gravity of Saturn in its vicinity. The index ∞ indicates quantities far from Saturn but at the same distance from the Sun. Using the two-body energy integral and the dust production rate at one of the moons, e.g. at Enceladus ($r = r_{\mathrm{E}}$), one can derive the r-dependence of the dust production rate (Krivov et al., 2003, and

references therein) at a certain E ring moon (index M)

$$N^+(>s, r_M) = N^+(>s, r_E)\frac{f_{imp}(r_M)}{f_{imp}(r_E)}\frac{Y_M}{Y_E}\frac{R_M^2}{R_E^2} \quad (13)$$

of grains larger in radius than s ejected in impacts of IDPs, with the normalized particle flux accounting for the gravitational focusing[1]

$$f_{imp}(r) = \sqrt{1+\frac{2GM_\hbar}{r(v_{imp}^\infty)^2}}\times\left\{\frac{1}{2}\sqrt{1+\frac{2GM_\hbar}{r(v_{imp}^\infty)^2}} + \frac{1}{2}\sqrt{1+\frac{2GM_\hbar}{r(v_{imp}^\infty)^2}-\left(\frac{R_\hbar}{r}\right)^2\left(1+\frac{2GM_\hbar}{R_\hbar(v_{imp}^\infty)^2}\right)}\right\}. \quad (14)$$

Here, the equatorial radius of Saturn is labeled by $R_\hbar$. The cumulative rate near Enceladus is found to be

$$N_{IDP}^+(>s, r_E) = 3.6\times10^{12}\left(\frac{s}{(1\,\mu m)}\right)^{-\gamma}(s^{-1}), \quad (15)$$

where $m_{imp} = 10^{-8}$ kg (corresponding to approx. $s_{imp} = 100\,\mu m$), $m_{max} \approx m_{imp}$, and the resulting yield according to Eq. (3) of $Y = 1.5\times10^4$ has been applied. With this, relation (9), where $v_0(\beta = 2) = 2.7\,m s^{-1}$ and $v_0(\beta = 3) = 29.9\,m s^{-1}$, yields the cumulative number of grains with radii larger than s and velocities $v > v_{esc}^{(E)} = 206.5\,m s^{-1}$ which escape Enceladus and contribute to the ring:

$$N_{IDP}^+(>v_{esc}^{(E)}, >s, r_E) \approx \begin{cases} 4.9\times10^{10}\left(\frac{s}{(1\,\mu m)}\right)^{-\gamma}(s^{-1}) & \text{for } \beta = 2, \\ 7.7\times10^{10}\left(\frac{s}{(1\,\mu m)}\right)^{-\gamma}(s^{-1}) & \text{for } \beta = 3. \end{cases} \quad (16)$$

Numerical values of N_{IDP}^+ have probably an order of magnitude or more uncertainty (Krivov et al., 2003). A comparison of the model predictions and Galileo measurements at Galilean satellites indicated that corresponding N_{IDP}^+ for Callisto, Europa, and Ganymede were systematically overestimated by a factor of 2–3 (Sremčević et al., 2005).

If the numbers (15) or (16), respectively, and the corresponding yield Y, could be specified by Cassini observations, Eqs. (9)–(13) are suitable to estimate the dust production by IDP impacts at the other E ring satellites. With these relations the number of particles (with radii larger than s) which may escape the gravity of the moon is

$$\frac{N_{IDP}^+(>v_{esc}^{(M)}, >s, r_M)}{N_{IDP}^+(>v_{esc}^{(E)}, >s, r_E)} = \left(\frac{v_0^{(M)}}{v_0^{(E)}}\frac{v_{esc}^{(E)}}{v_{esc}^{(M)}}\right)^{\beta-1}\frac{f_{imp}(r_M)}{f_{imp}(r_E)}\frac{R_M^2}{R_E^2}\frac{Y_M}{Y_E}, \quad (17)$$

where the escape velocity of the satellite is denoted by $v_{esc}^{(M)}$.

2.3. E ring impactors—ERPs

In addition to the IDP projectiles we need to estimate the mass flux of E ring impactors $F_{imp}(r) = \langle m_{imp}\rangle n_{imp}(r)\langle v_{imp}\rangle(r)$ as a function of distance from Saturn r in the equatorial plane. To this end, we need a model for the configuration of particles in the E ring. For simplicity, we employ results from the modeling of Voyager observations derived by Showalter et al. (1991) (see also Juhász and Horányi, 2002)

$$n_{imp}(r) = n_{imp}(r_E)\frac{\langle H\rangle(r_E)}{\langle H\rangle(r)}\begin{cases}\left(\frac{r}{r_E}\right)^{15} & \text{for } r<r_E, \\ \left(\frac{r}{r_E}\right)^{-7} & \text{for } r>r_E,\end{cases} \quad (18)$$

with the particle number density near Enceladus $n_{imp}(r_E) \approx 1\,m^{-3}$ and the mean vertical width $\langle H\rangle(r_E) \approx 8\times10^3$ km up to about $\langle H\rangle \approx 2\times10^4$ km near Rhea. For the mean impact speed we assume that $s\sim0.65\,\mu m$ E ring motes coming from Enceladus quickly develop large eccentricities, until they are absorbed by the A ring or the E ring moons after only a few years. Then, following Hamilton and Burns (1994), the mean impact velocity with the E ring satellites can be estimated as

$$\langle v_{imp}\rangle \approx \langle e\rangle v_K(r_M) \quad \text{with } v_K(r_M) = \sqrt{\frac{GM_\hbar}{r_M}}, \quad (19)$$

with the mean eccentricity $\langle e\rangle \approx 0.5$.

The applicability of Eq. (19) is discussed in this paragraph using data from a simulation (Fig. 2). The evolution of one particle launched at Enceladus is simulated for two Saturnian years, subject to gravitational, electromagnetic and radiation forces which are plausible for the E-ring region (Horányi et al., 1992). The equilibrium potential of the particle is assumed to follow a form suggested by recent Cassini data (Kempf et al., 2006; Wahlund et al., 2005), ranging from about -2 to -3 V between 3 to $4R_\hbar$ with a transition to positive values between 6 and $8R_\hbar$ to an approximately constant value of about $+5$ V outside $10R_\hbar$. In this case, particles of a radius near 0.65 μm most rapidly develop eccentricities as high as 0.6–0.7. The lower left panel in the figure shows the relative velocity v_{rel} of the dust particle in the simulation with respect to the velocity of a circular Keplerian orbit (labeled in the plot by v_K) at the instantaneous radial position r (stored equidistantly in time) of the particle. When plotted vs the instantaneous eccentricities of the particle the linear

[1] Colombo et al. (1966) have a misprint in their Eq. (11). Evaluating their Eq. (7) actually results in Eq. (14) above which we verified using different methods.

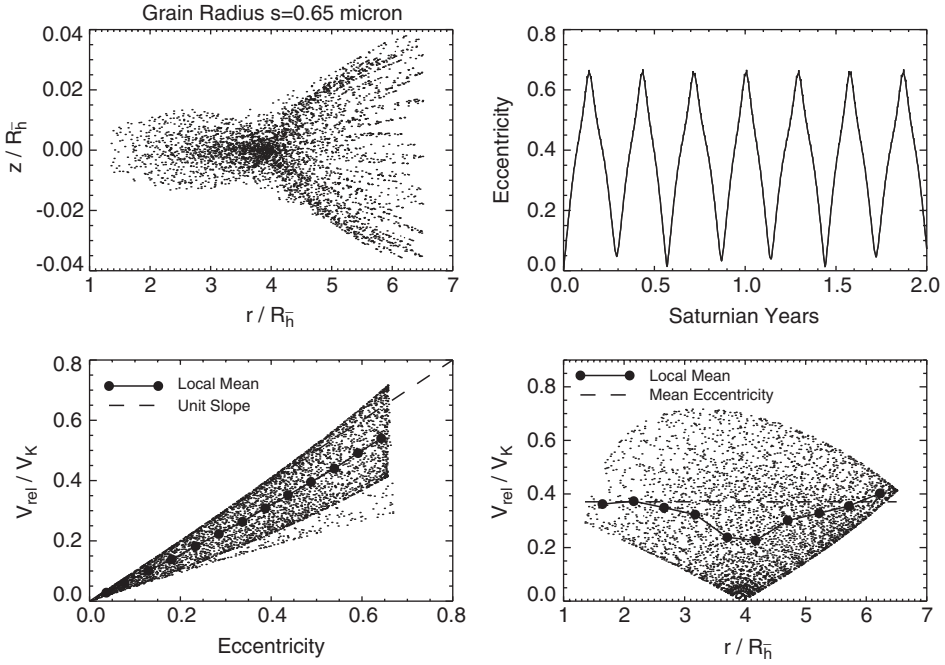

Fig. 2. Simulation of a dust particle launched on the orbit of Enceladus. *Upper left panel*: scatter plot of height z of the particle above the equatorial plane vs radial distance from Saturn r. *Upper right*: evolution of the particle eccentricity. *Lower left*: ratio of the particle velocity relative to a circular Keplerian orbit at the instantaneous particle position vs the instantaneous eccentricity. *Lower right*: particle velocity relative to a circular Keplerian orbit normalized by the circular Keplerian orbit vs instantaneous radial position.

trend of Eq. (19) is clearly visible. The lower right panel of Fig. (2) shows that ratio $v_{\rm rel}/v_{\rm K}$ plotted vs the instantaneous radial particle position. For all radial positions reached by the particle the local mean of this velocity ratio is indeed on the order of the total mean eccentricity. A qualitatively similar behavior is observed in simulations with different grain sizes, for different forms of the electromagnetic equilibrium potential, or, if particle sinks, plasma drag, and the gravity of the moons are included in the simulation.

With Eqs. (18) and (19) the particle creation at Enceladus caused by 0.65 μm E ring projectiles ($\langle m_{\rm imp}\rangle = 2.3\times10^{-15}$ kg) with a yield $Y = 25.3$ according to Eq. (3) is found to be

$$N^{+}_{\rm ERP}(>s, r_{\rm E}) = 1.2\times10^{14}\left(\frac{s}{(1\,\mu{\rm m})}\right)^{-\gamma}({\rm s}^{-1}). \tag{20}$$

The fraction of ejected particles

$$N^{+}_{\rm ERP}(>v^{(\rm E)}_{\rm esc}, >s, r_{\rm E}) = \begin{cases} 1.5\times10^{13}\left(\frac{s}{(1\,\mu{\rm m})}\right)^{-\gamma}({\rm s}^{-1}) & \text{for } \beta = 2, \\ 3.3\times10^{13}\left(\frac{s}{(1\,\mu{\rm m})}\right)^{-\gamma}({\rm s}^{-1}) & \text{for } \beta = 3 \end{cases} \tag{21}$$

can escape Enceladus' vicinity (Eq. (9) for $v_0(\beta=2) = 26.5\,{\rm ms}^{-1}$ and $v_0(\beta=3) = 109.0\,{\rm ms}^{-1}$) and support the E ring. Varying the radius of the impacting E ring projectiles for $s\in[0.5; 1.0; 2.0]\,\mu$m and the mean eccentricity between $\langle e\rangle \in [0.25; 0.5]$ did result in changes of $N^{+}_{\rm ERP}$ of one order of magnitude or more. For instance, a power law distribution in the range $s\in[0.3\cdots3]\,\mu$m (Nicholson et al., 1996; Juhász and Horányi, 2002) gives larger rates, whereas a narrow distribution around $s\approx1\pm0.3\,\mu$m (Showalter et al., 1991) reduces it by an order of magnitude. Similar to Eq. (17) the dust production rate for the ERP at different E ring moons may be written as

$$\frac{N^{+}_{\rm ERP}(>v^{(\rm M)}_{\rm esc}, >s, r_{\rm M})}{N^{+}_{\rm ERP}(>v^{(\rm E)}_{\rm esc}, >s, r_{\rm E})} = \left(\frac{v^{(\rm M)}_0}{v^{(\rm E)}_0}\frac{v^{(\rm E)}_{\rm esc}}{v^{(\rm M)}_{\rm esc}}\right)^{\beta-1}\frac{n_{imp}(r_{\rm M})}{n_{imp}(r_{\rm E})}\frac{v_{\rm K}(r_{\rm M})}{v_{\rm K}(r_{\rm E})}\frac{R^2_{\rm M}}{R^2_{\rm E}}\frac{Y_{\rm M}}{Y_{\rm E}}. \tag{22}$$

3. Results and discussion

In the following we will use the CDA/HRD measurements performed during the Cassini–Enceladus flyby E11 on July 14, 2005 in order to estimate the different contributions of impactor-ejecta created dust at various satellites embedded in the E ring. In the subsequent subsections, we will

(1) briefly summarize the approach applied by Spahn et al. (2006) for the Enceladus flyby;
(2) compare the observational results with the impactor-ejecta rates;
(3) apply the impactor-ejecta model concerning ERPs and IDPs to all satellites embedded in the E ring and discuss the consequences.

3.1. Dust production rates at Enceladus from Cassini-HRD measurements

The left panel of Fig. 3 shows contours of particle density in Enceladus' vicinity simulated for isotropic ejection of grains from Enceladus' surface. The dynamics of freshly ejected grains has been tracked until they meet one of the E ring sinks. The phase-space variables have then been stored equidistantly in time mimicking a steady single particle distribution. In this way the E ring background has been modeled where in Fig. 3 only particles with radii $s>2\,\mu m$ have been counted, in accordance with the HRD threshold. Superposing the freshly ejected fluxes with those of the E ring background we have calculated the dust impact rates expected at the HRD along the Cassini trajectory (E11) as a function of time. It turned out, that the dust launched by the impactor-ejecta process causes impact rates at the dust detector which are symmetric with respect to the time of the closest approach (C/A), independently of the type of the projectile family. Thus, the dust impact rate at the CDA/HRD is expected to peak at C/A. This result of the modeling has then been compared to the HRD data (diamonds). This flyby has provided a particularly good chance to identify the location of dust sources at the satellites' surface since the spacecraft pierced deeply through the Hill sphere of Enceladus.

Surprisingly, the dust impact-rate at the HRD has shown a maximum almost a minute before the C/A contradicting our expectations based upon impact-created dust cloud. An efficient dust source at the south pole of Enceladus offers a solution of this inconsistency (Brown et al., 2006; Hansen et al., 2006; Jones et al., 2006; Spahn et al., 2006). Our fit to the data has yielded the following absolute dust ejection rates:

$$N^{+}_{\mathrm{south}}(>v^{(\mathrm{E})}_{\mathrm{esc}},>2\,\mu m,r_{\mathrm{E}})\approx 5\times 10^{12}\ (\mathrm{s}^{-1}) \tag{23}$$

for the south-pole source and

$$N^{+}_{\mathrm{impact}}(>v^{(\mathrm{E})}_{\mathrm{esc}},>2\,\mu m,r_{\mathrm{E}})<1\times 10^{12}\,(\mathrm{s}^{-1}) \tag{24}$$

for the impact-generated dust. The latter number is to be compared to the ejecta rates (16) and (21), applying a correction factor of $2^{-\gamma}\approx 0.2$ accounting for larger grains ($s\geqslant 2\,\mu m$) detectable with the HRD.

3.2. Comparison of the measured and predicted rates at Enceladus

Firstly, the number (24) accounts for both kinds of projectiles, IDPs and ERPs, creating dust by their impacts, i.e. it is a superposition of both contributions

$$N^{+}_{\mathrm{impact}}=N^{+}_{\mathrm{ERP}}+N^{+}_{\mathrm{IDP}}. \tag{25}$$

However, which of both contributions, N^{+}_{ERP} or N^{+}_{IDP}, dominates the dust generated by impactors cannot be judged from the single flyby E11 of Cassini at Enceladus. Our estimates (16) and (21) indicate that the dust production caused by the IDPs is less efficient by a factor of 10^{-2} mainly due to the very large E ring flux compared to the IDPs. ERPs seem to dominate the creation of E ring grains near Enceladus, of course, in addition to the most efficient source at the south pole.

The questions remain: is there a possibility to discriminate between contributions ejected by the ERPs and the IDPs? And, can parameters characterizing the impactor-ejecta model be gauged using the HRD result obtained during the E11 flyby?

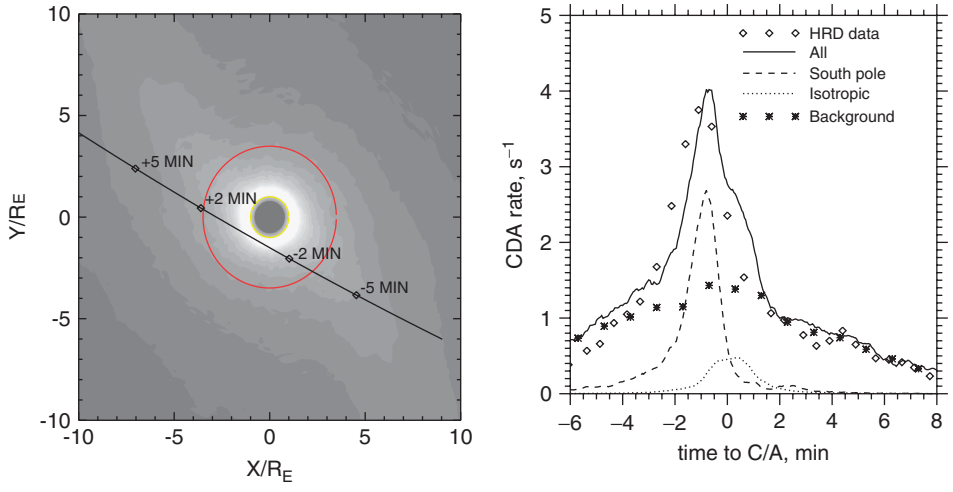

Fig. 3. *Left panel*: Contours of equal particle density in Enceladus' vicinity in the equatorial plane (x points radially outward, y in orbit direction). This dust configuration is produced by an isotropic distribution of dust sources on the satellite. A projection of the Cassini trajectory during the flyby E11 (14 July 2005) onto the plane is shown. The spacecraft crosses the plane from south. *Right*: HRD data (diamonds) and a fit from simulated dust configurations in the moon's vicinity. The model rate which is composed of south-pole dust (dashed line), grains launched by the impactor-ejecta process (dotted curve), and the E ring background (stars). For the simulation of the latter 1 μm particles have been chosen which are subject to the perturbations Saturn's oblateness, Lorentz force and radiation pressure force. The ratio between rate of the south-pole source and the impactor-ejecta generated one are chosen such that no secondary peak develops in the combined profile directly at C/A.

In order to compare the model and the measured HRD rates, we recall the dust production numbers (16) and (21) at Enceladus for grains larger than $s = 2\,\mu m$

$$N^{+}_{IDP}(>v^{(E)}_{esc}, >2\,\mu m) \approx \begin{cases} 9.2\times10^{9}\,(s^{-1}) & \text{for } \beta = 2, \\ 1.5\times10^{10}\,(s^{-1}) & \text{for } \beta = 3, \end{cases} \quad (26)$$

$$N^{+}_{ERP}(>v^{(E)}_{esc}, >2\,\mu m) \approx \begin{cases} 2.8\times10^{12}\,(s^{-1}) & \text{for } \beta = 2, \\ 6.2\times10^{12}\,(s^{-1}) & \text{for } \beta = 3. \end{cases} \quad (27)$$

Table 1
Physical properties of embedded satellites within Saturn's E ring

Satellite	r/R_h	M (10^{20} kg)	R (km)	v_{esc} (m s^{-1})
Mimas	3.3	0.4	198.8	127.2
Enceladus	4.1	1.1	252.3	204.8
Tethys	5.1	6.2	536.3	338.3
Dione	6.5	11.0	563.0	462.7
Rhea	9.1	23.1	765.5	591.8

v_{esc} is the three-body escape velocity according to Eq. (8).

In view of these rough estimates the rates caused by E ring impactors at Enceladus meet the observations (Spahn et al., 2006) fairly well so that the relation defining the yield (3) specifies obviously essential aspects of dependence on the impactors mass m_{imp} and impact speed v_{imp}. Further, the ERPs dominate the impactor generated creation of dust at Enceladus compared to that of the IDPs— by a factor of 100. Does this also apply to the other satellites embedded in the E ring?

3.3. Dust production rates at different moons

A comparison of the dust production rates N^{+}_{IDP} and N^{+}_{ERP} at the E ring moons from Mimas to Rhea (physical properties are given in Table 1) is presented in the Table 2. Values are based on Eq. (16) and (17) for the IDPs and Eqs. (21) and (22) for the ERPs. Values marked with (∗) are normalized to the corresponding value at Enceladus.

There is a clear difference in the dust production rates between the two projectile families—ERPs and IDPs. Whereas the ejecta created by the ERPs are only significant at Enceladus and perhaps at Tethys, the other satellites do

Table 2
Model parameters and calculated values for IDPs and ERPs

Scenario	Parameter	Eq.	Mimas	Enceladus	Tethys	Dione	Rhea
	$f_{imp}(r_M)$	(14)	5.0	4.3	3.7	3.1	2.5
	F_{imp} (10^{-15} kg m^{-2} s^{-1})	(1)	0.89	0.77	0.67	0.56	0.46
	Y	(3)	18,000	15,000	12,000	9,800	7,500
	N^{+} (10^{12} s^{-1})	(4)	3.2	3.6	12.0	8.7	10.0
	$v_0(\beta = 2)$ (m s^{-1})	(7)	2.6	2.7	2.8	3.0	3.1
IDP	$N^{+}(>v_{esc};\beta = 2)$ (10^{10} s^{-1})	(9)	6.6	4.9	9.7	5.6	5.3
	$M^{+}(>v_{esc};\beta = 2)$ (kg s^{-1})	(10)	0.042	0.031	0.062	0.035	0.033
	$v_0(\beta = 3)$ (m s^{-1})	(7)	29	30	30	31	32
	$N^{+}(>v_{esc};\beta = 3)$ (10^{10} s^{-1})	(9)	17.0	7.7	9.4	3.9	2.9
	$M^{+}(>v_{esc};\beta = 3)$ (kg s^{-1})	(10)	0.11	0.049	0.060	0.025	0.019
	$N^{+}(>v_{esc};\beta = 2)(*)$	(17)	1.4	1.0	2.0	1.1	1.1
	$N^{+}(>v_{esc};\beta = 3)(*)$	(17)	2.2	1.0	1.2	0.5	0.4
	$n_{imp}(r_M)$ (m^{-3})	(18)	0.03	1.0	0.2	0.02	0.002
	F_{imp} (10^{-15} kg m^{-2} s^{-1})	(1)	620	15,000	2,300	270	15
	Y	(3)	33	25	19	14	10
	N^{+} (10^{12} s^{-1})	(4)	3.9	120.0	63.0	6.0	0.41
	$v_0(\beta = 2)$ (m s^{-1})	(7)	25	26	28	29	32
ERP	$N^{+}(>v_{esc};\beta = 2)$ (10^{10} s^{-1})	(9)	78	1,500	520	38	2.2
	$M^{+}(>v_{esc};\beta = 2)$ (kg s^{-1})	(10)	0.50	9.5	3.3	0.24	0.014
	$v_0(\beta = 3)$ (m s^{-1})	(7)	106	109	112	116	121
	$N^{+}(>v_{esc};\beta = 3)$ (10^{10} s^{-1})	(9)	270	3,300	690	37	1.7
	$M^{+}(>v_{esc};\beta = 3)$ (kg s^{-1})	(10)	1.7	21.0	4.4	0.24	0.011
	$N^{+}(>v_{esc};\beta = 2)(*)$	(22)	0.05	1.0	0.3	0.03	0.001
	$N^{+}(>v_{esc};\beta = 3)(*)$	(22)	0.08	1.0	0.2	0.01	0.0005
	$F^{ERP}_{imp}/F^{IDP}_{imp}$ (10^3)		0.69	19.0	3.4	0.47	0.033
IDP	Y_{ERP}/Y_{IDP} (10^{-3})		1.8	1.7	1.6	1.5	1.3
vs	N^{+}_{ERP}/N^{+}_{IDP}		1.2	32.0	5.4	0.69	0.041
ERP	$N^{+}_{ERP}/N^{+}_{IDP}(>v_{esc})$ $(\beta = 2)$		12.0	310.0	53.0	6.8	0.42
	$N^{+}_{ERP}/N^{+}_{IDP}(>v_{esc})$ $(\beta = 3)$		16.0	420.0	73.0	9.5	0.59

(∗) denotes values normalized to respective Enceladus' values.

practically not contribute to the E ring dust. In the E ring outskirts the IDPs dust contribution is comparable and even exceeds the ERP production. However, one has to remember that the total share of dust creation beyond Dione is less than 1% and that the majority of the dust comes from Enceladus and Tethys. Nevertheless, even such a small dust supply in the outer E ring, driven to great extent by IDPs, might help to understand the large radial extent of the E ring.

These relatively large differences in the dust production efficiency caused by ERPs at the other moons in the E ring furnish an opportunity to discriminate between the two impactor classes. To this aim, further close Cassini flybys of the satellites embedded in the E ring, including Enceladus, are necessary. Especially, more flybys of Enceladus would be beneficial in order to study the nature of the south-pole source as well as the dust production caused by the "classical" impactor-ejecta mechanism.

In Table 2 we list the total mass production rate $M^+(>v_{esc})$ for IDPs and ERPs. The combined $M^+(>v_{esc})$ for IDPs is $\sim 0.1\,\mathrm{kg\,s^{-1}}$, while for ERPs it is $\sim 10\,\mathrm{kg\,s^{-1}}$. Based on the analysis of Voyager data, Juhász and Horányi (2002) give an estimate of $\sim \mathrm{kg\,s^{-1}}$ required to fit the observations for grain sizes of $s \in [0.1, 2.2]\,\mu\mathrm{m}$. Calculating $M^+(s \in [s_1, s_2]) = ((s_2/s_{\max})^{3-\gamma} - (s_1/s_{\max})^{3-\gamma})$ $M^+ \approx 0.1 M^+$ gives $\sim 2\,\mathrm{kg\,s^{-1}}$ for ERPs which is consistent with Voyager data.

It is interesting to emphasize that Tethys obviously serves as the second efficient dust source of the E ring (see Table 2) supporting the Earth-based observations with the W. M. Keck telescope by de Pater et al. (2004) during the ring plane crossing of the Earth in summer 1995.

4. Conclusions

In this paper we have investigated the role of the impactor-ejecta process for the dust production at satellites embedded in the E ring of Saturn. The study is based on the dust measurements during Cassini's Enceladus flyby E11 which have tightly constrained the rates of dust production by a source near the moon's south pole, as well as by hypervelocity impacts (Spahn et al., 2006). The latter rate has been compared to models describing the impactor-ejecta process driven by two impactor families: the E ring particles (ERPs) themselves and interplanetary dust projectiles (IDPs). In particular, the yield Y and the flux $F_{\mathrm{imp}}^{\mathrm{IDP}}$ specified in Krivov et al. (2003) are found to be consistent with the E11 data.

Further, the impactor-ejecta model has been applied to both impactor families hitting other satellites embedded in the E ring. Significant differences have been obtained for the dust production efficiencies at these moons, as summarized in Tables 1 and 2. The inner region of the E ring (from Mimas to Tethys), where the highest densities are observed, is sustained by Enceladus' south-pole dust source and by ejecta due to ERP, in approximately 5:1 ratio. The dust production by IDPs is by a factor of 100 less efficient than that by the ERPs. Further out, the dust production efficiency by ERPs reduces, while the IDPs produce a comparable amount of dust at all E ring moons. For instance, at Dione the production rates caused by ERPs and IDPs become close. At Rhea the dust production caused by ERPs is reduced by three orders of magnitude compared to that at Enceladus. This means that at Rhea about 10 times more dust can be expected to be produced by IDPs than by ERPs.

Thus, it seems likely that both impactor classes play their role in sustaining the E ring. The IDP contribution dominates the particle production in the outer E ring, possibly explaining the large radial extent of the ring, whereas ERP impacts (and the Enceladus south-pole source, of course) play crucial role in the inner region.

The differences in the predicted dust production rates due to IDPs and ERPs at various moon locations can be verified in future flybys of the Cassini spacecraft with E ring satellites.

Acknowledgments

The authors wish to thank Antal Juhász and an anonymous referee for the helpful comments in making the paper more convincing. The work has been supported by the *Deutsche Forschungsgemeinschaft (DFG)*: Grants Sp 384/17-2 and Sp 384/18-3, by the *Zentrum für Luft- und Raumfahrt (DLR)*: Grants 50 OH 0003 and 500 OH 91019, and by the *Cassini-UVIS*-project.

References

Brown, R.H., Clark, R.N., Buratti, B.J., Cruikshank, D.P., Barnes, J.W., Mastrapa, R.M.E., Bauer, J., Newman, S., Momary, T., Baines, K.H., Bellucci, G., Capaccioni, F., Cerroni, P., Combes, M., Coradini, A., Drossart, P., Formisano, V., Jaumann, R., Langevin, Y., Matson, D.L., McCord, T.B., Nelson, R.M., Nicholson, P., Sicardy, B., Sotin, C., 2006. Composition and physical properties of Enceladus' surface from Cassini's visual and infrared mapping spectrometer. Science 311, 1425–1428.

Colombo, G., Lautman, D.A., Shapiro, I.I., 1966. The Earth's dust belt: fact or fiction? 2. Gravitational focusing and Jacobi capture. J. Geophys. Res. 71, 5705–5717.

Colwell, J.E., 1993. A general formulation for the distribution of impacts and ejecta from small planetary satellites. Icarus 106, 536–548.

de Pater, I., Martin, S., Showalter, M.R., 2004. Keck near-infrared observations of Saturn's E and G rings during Earth's ring plane crossing in August 1995. Icarus 172, 446–454.

Divine, N., 1993. Five populations of interplanetary meteoroids. J. Geophys. Res. 98, 17029–17048.

Hamilton, D.P., Burns, J.A., 1994. Origin of Saturn's E ring: self-sustained, naturally. Science 264, 550–553.

Hansen, C.J., Hendrix, A.R., West, R.A., Esposito, L.W., Stewart, A.I.F., Shemansky, D.E., Pryor, W., 2006. Cassini ultraviolet imaging spectrograph (UVIS) investigation of Enceladus' water vapor plume. Science 311, 1422–1425.

Horányi, M., Burns, J.A., Hamilton, D.P., 1992. The dynamics of Saturn's E ring particles. Icarus 97, 248–259.

Housen, K.R., 1991. Laboratory simulations of large-scale fragmentation events. Icarus 94, 180–190.

Housen, K.R., Schmidt, R.M., Holsapple, K.A., 1983. Crater ejecta scaling laws—fundamental forms based on dimensional analysis. J. Geophys. Res. 88, 2485–2499.

Jones, G.H., Roussos, E., Krupp, N., Paranicas2, C., Woch, J., Lagg, A., Mitchell, D.G., Krimigis, S.M., Dougherty, M.K., 2006. Enceladus's varying imprint on the Kronian magnetosphere. Science 311, 1412–1415.

Juhász, A., Horányi, M., 2002. Saturn's E ring: a dynamical approach. J. Geophys. Res. 107, doi:10.1029/2001JA000182.

Kempf, S., Beckmann, U., Srama, R., Horányi, M., Auer, S., Grün, E. 2006. The electro-static potential of E ring particles. Planet. Space Sci., submitted for publication.

Koschny, D., Grün, E., 2001. Impacts into ice-silicate mixtures: crater morphologies volumes depth-to-diameter ratios, and yield. Icarus 154, 391–401.

Krivov, A.V., Sremčević, M., Spahn, F., Dikarev, V.V., Kholshevnikov, K.V., 2003. Impact-generated dust clouds around planetary satellites: spherically symmetric case. Planet. Space Sci. 51, 251–269.

Krivov, A. V., Feofilov, A. G., Dikarev, V. V., 2006. Search for the putative dust belts of Mars: the late 2007 opportunity. Planet. Space Sci., this issue.

Makuch, M., Brilliantov, N. V., Sremcevic, M., Spahn, F., Krivov, A. V., 2006. Stochastic circumplanetary dynamics of rotating non-spherical dust particles. Planet. Space Sci., this issue.

Nicholson, P.D., Showalter, M.R., Dones, L., French, R.G., Larson, S.M., Lissauer, J.J., McGhee, C.A., Sicardy, B., Seitzer, P., Danielson, G.E., 1996. Observations of saturn's ring-plane crossing in August and November 1995. Science 272, 509–516.

Porco, C., Helfenstein, P., Thomas, P., Ingersoll, A.P., Wisdom, J., West, R., Neukum, G., Denk, T., Wagner, R., Roatsch, T., Kieffer, S., Turtle, E., McEwen, A., Johnson, T., Rathbun2, J., Veverka, J., Wilson, D., Perry, J., Spitale, J., Brahic, A., Burns, J., DelGenio, A., Dones, L., Murray, C., Squyres, S., 2006. Cassini images the active south pole of Enceladus. Science 311, 1393–1401.

Showalter, M.R., 1998. Detection of centimeter-sized meteoroid impact events in Saturn's F ring. Science 282, 1099–1102.

Showalter, M., Cuzzi, J., Larson, S., 1991. Structure and particle properties of Saturn's E ring. Icarus 94, 451–473.

Showalter, M. R., Hamilton, D. P., Nicholson, P. D., 2006. A deep search for Martian dust rings and inner moons using the Hubble space telescope. Planet. Space Sci., this issue.

Soter, S., 1971. The dust belts of Mars. Technical Report, Center for Radiophysics and Space Research.

Spahn, F., Thiessenhusen, K.-U., Colwell, J.E., Srama, R., Grün, E., 1999. Dynamics of dust ejected from Enceladus: application to the Cassini dust detector. J. Geophys. Res. 104, 24111–24120.

Spahn, F., Schmidt, J., Albers, N., Hörning, M., Makuch, M., Seiß, M., Kempf, S., Srama, R., Dikarev, V.V., Helfert, S., Moragas-Klostermeyer, G., Krivov, A.V., Sremčević, M., Tuzzolino, A., Economou, T., Grün, E., 2006. Cassini dust measurements at Enceladus: implications for Saturn's E ring. Science 311, 1416–1418.

Spencer, J. R., Pearl, J. C., Segura, M., Flasar, F. M., Mamoutkine, A., Romani, P., Buratti, B. J., Hendrix, A. R., Spilker, L. J., Lopes, R. M. C., 2006. Cassini encounters Enceladus: background and the discovery of a south polar hot spot. Science 311, 1401–1405.

Sremčević, M., Krivov, A.V., Spahn, F., 2003. Impact generated dust clouds around planetary satellites: asymmetry effects. Planet. Space Sci. 51, 455–471.

Sremčević, M., Krivov, A.V., Krüger, H., Spahn, F., 2005. Impact generated dust clouds around planetary satellites: model versus Galileo data. Planet. Space Sci. 53, 625–641.

Wahlund, J.-E., Boström, R., Gustafsson, G., Gurnett, D.A., Kurth, W.S., Averkamp, T., Hospodarsky, G.B., Persoon, A.M., Canu, P., Pedersen, A., Desch, M.D., Eriksson, A.I., Gill, R., Morooka, M.W., André, M., 2005. The inner magnetosphere of Saturn: Cassini RPWS cold plasma results from the first encounter. Geophys. Res. Lett. 32, doi:10.1029/2005GL022699.

Waite Jr., J. H., Combi, M.R., Ip, W.-H., Cravens, T. E., McNutt Jr., R. L., Kasprzak, W., Yelle, R., Luhmann, J., Niemann, H., Gell, D., Magee, B., Fletcher, G., Lunine, J., Tseng, W.-L., 2006. Cassini ion and neutral mass spectrometer: enceladus plume, composition and structure. Science 311, 1419–1422.